THE JOURNAL OF BIOLOGICAL CHEMISTRY VOL. 291, NO. 35, pp. 18210–18221, August 26, 2016

Endogenous N-terminal Domain Cleavage Modulates α_{1D}-Adrenergic Receptor Pharmacodynamics*[S]

Received for publication, March 25, 2016, and in revised form, June 30, 2016 Published, JBC Papers in Press, July 5, 2016, DOI 10.1074/jbc.M116.729517

Timothy S. Kountz[‡1], Kyung-Soon Lee[‡], Stacey Aggarwal-Howarth[‡§2], Elizabeth Curran[‡], Ji-Min Park[‡], Dorathy-Ann Harris[‡3], Aaron Stewart[‡1], Joseph Hendrickson[‡], Nathan D. Camp[¶4], Alejandro Wolf-Yadlin[¶], Edith H. Wang[‡], John D. Scott[‡§], and Chris Hague[‡5]

From the [§]Howard Hughes Medical Institute and the Departments of [‡]Pharmacology and [¶]Genome Sciences, University of Washington School of Medicine, Seattle, Washington 98195

The α_{1D}-adrenergic receptor (ADRA1D) is a key regulator of cardiovascular, prostate, and central nervous system functions. This clinically relevant G protein-coupled receptor has proven difficult to study, as it must form an obligate modular homodimer containing the PDZ proteins scribble and syntrophin or become retained in the endoplasmic reticulum as nonfunctional protein. We previously determined that targeted removal of the N-terminal (NT) 79 amino acids facilitates ADRA1D plasma membrane expression and agonist-stimulated functional responses. However, whether such an event occurs in physiological contexts was unknown. Herein, we report the ADRA1D is subjected to innate NT processing in cultured human cells. SNAP near-infrared imaging and tandem-affinity purification revealed the ADRA1D is expressed as both full-length and NT truncated forms in multiple human cell lines. Serial truncation mapping identified the cleavage site as Leu^{90}/Val^{91} in the 95-amino acid ADRA1D NT domain, suggesting human cells express a Δ1–91 ADRA1D species. Tandem-affinity purification MS/MS and co-immunoprecipitation analysis indicate NT processing of ADRA1D is not required to form scribble-syntrophin macromolecular complexes. Yet, label-free dynamic mass redistribution signaling assays demonstrate that Δ1–91 ADRA1D agonist responses were greater than WT ADRA1D. Mutagenesis of the cleavage site nullified the processing event, resulting in ADRA1D agonist responses less than the WT receptor. Thus, we propose that processing of the ADRA1D NT domain is a physiological mechanism employed by cells to generate a functional ADRA1D isoform with optimal pharmacodynamic properties.

α_1-Adrenergic receptors (ARs)[6] belong to the superfamily of class A G protein-coupled receptors (GPCRs). Stimulated by the endogenous catecholamines norepinephrine and epinephrine, α_1-ARs help coordinate sympathetic nervous function along with the α_2- and β-AR subtypes. This mode of GPCR signaling is particularly relevant during stress, exercise, or life-threatening situations, as it permits an organism to respond to environmental stimuli supra-maximally and thereby enhance survival probability.

Significant gaps remain in our understanding of α_1-AR biology. Of particular note is the α_{1D}-AR subtype (ADRA1D). Unlike the closely related α_{1A} (ADRA1A) and α_{1B} (ADRA1B) subtypes, which achieve significant plasma membrane expression and robustly respond to agonists in cultured cells, the ADRA1D is cumbersome to study *in vitro* (1). Following its initial cloning and pharmacological characterization (2–4), numerous studies revealed the ADRA1D is sequestered intracellularly in myriad cell lines (5–11), where it has limited access to agonists and displays minimal functional activity. In a key study, Fan *et al.* (12) demonstrated ADRA1D functional expression is lost in cultured aortic vascular muscle cells ~48 h post-dissection. They concluded that factors required for ADRA1D functional expression *in vivo* are absent in cell culture conditions (12), which may explain why human cell lines expressing detectable levels of functional ADRA1D are lacking.

Thus, our current knowledge of the molecular and cellular mechanisms that govern the activity of this clinically relevant GPCR is inadequate and incomplete. Indeed, numerous clinical observations indicate the ADRA1D plays an essential role in bladder (13–15), prostate (16, 17), and coronary artery (18) function, central nervous system processes (19–21), blood pressure regulation (22, 23), and possibly cancer (24). Thus, understanding the molecular mechanisms by which the ADRA1D functions in human cells may open new avenues of therapeutic development and drug discovery.

Recently, we and others have begun to unravel this ADRA1D mystery. A discriminating feature of the α_1-subtypes is the length of the extracellular N terminus (NT). The ADRA1A is 15 amino acids and ADRA1B is 35, whereas the NT domain of ADRA1D is unusually long for class A GPCRs at 95 amino acids.

* This work was supported in part by National Institutes of Health Grants RO1 GM100893 (to C. H.) and DK054441 and DK105542 (to J. D. S.). The authors declare that they have no conflicts of interest with the contents of this article. The content is solely the responsibility of the authors and does not necessarily represent the official views of the National Institutes of Health.
[S] This article contains supplemental Tables S1 and S2 and Figs. S1–S3.
[1] Mary Gates University of Washington Research Scholars.
[2] Supported in part by National Institutes of Health, USPHS, National Research Service Award, T32GM007270.
[3] Ronald E. McNair Scholar.
[4] Supported by National Institutes of Health Human Genome Research Institute Grant T32 HG00035.
[5] To whom correspondence should be addressed: Dept. of Pharmacology, University of Washington School of Medicine, 1959 Pacific Ave., Box 357280, Seattle, WA 98195. Tel.: 206-221-4612; E-mail: chague@uw.edu.

[6] The abbreviations used are: AR, adrenergic receptor; ADRA1A, α_{1A}-adrenergic receptor; ADRA1B, α_{1B}-adrenergic receptor; ADRA1D, α_{1D}-adrenergic receptor; DMR, dynamic mass redistribution; NT, N-terminal; TAP, tandem-affinity purification; ER, endoplasmic reticulum; GPCR, G protein-coupled receptor; IA, intrinsic activity.

Previous studies revealed truncating the proximal 79 amino acids of the NT liberates ADRA1D from intracellular clusters, facilitates trafficking to the plasma membrane, and enhances functional coupling in response to agonist stimulation (25–27). Although a useful experimental approach, no data existed suggesting the ADRA1D NT is subjected to post-translational proteolysis *in situ* or occurred under physiological contexts.

Here, we report the unexpected finding that the proximal 91 amino acids of the ADRA1D NT are removed when the proreceptor is expressed in cultured human cells.

Results

ADRA1D N-terminal Domain Is Endogenously Cleaved in Human Cells—A variety of biochemical and pharmacological assays have been used to identify and deconvolute α_1-adrenergic receptor (AR) macromolecular complexes in living cells (23, 28, 29). One over-riding experimental limitation has been the lack of sufficiently specific anti-α_1-AR antibodies. Most, if not all, of the commercially available anti-α_1-AR antibodies generate non-specific artifacts and/or false-positive results, as demonstrated by rigorous Western blotting analysis performed on various tissues isolated from WT and combinations of single, double, and triple α_1-AR knock-out mice (30). Coupled with the lack of human cell lines that express functional α_{1D}-AR (ADRA1D), these experimental roadblocks require alternative technological approaches to study the molecular and cellular properties of α_1-ARs.

Thus, we employed SNAP-tag technology, as this innovative protein epitope tag eliminates the need for antibodies. Protein detection is achieved by chemical cross-linking of fluorescent benzylguanine derivatives, permitting direct imaging of protein bands in the polyacrylamide gel (31).

Accordingly, the three human α_1-AR subtypes were subcloned into the pSNAP vector to add N-terminal human O^6-alkylguanine-DNA alkyltransferase (SNAP) epitope tags. Each SNAP α_1-AR was transfected into HEK293T cells and imaged on a polyacrylamide gel in the 700–800 nm wavelength range using LI-COR Odyssey. Monomeric entities were detected for all α_1-AR species, as well as dimers/oligomers at higher molecular weights (Fig. 1*A*). Unexpectedly, a dense band migrating at ~30–35 kDa was detected in the *ADRA1D lane* (Fig. 1*A*). After subtracting the SNAP tag and linker region (25 kDa) from full-length SNAP-ADRA1D species (80.3 kDa), this band is roughly equivalent in size to the 8.2-kDa 95-amino acid ADRA1D N terminus (NT).

Multiple alternative approaches validated this result (schematic of epitope-tagged ADRA1D constructs shown in Fig. 1*F*). NT tandem affinity purification (TAP)-tagged ADRA1D (72.2 kDa) was isolated from digitonin-solubilized HEK293T cell lysates with streptavidin beads, examined via silver stain (Fig. 1*B*) and anti-HA immunoblotting (Fig. 1*C*). Again, an ~30–35-kDa band was detected in the biotin-bound fraction (Fig. 1, *B* and *C*, *4th lane, Beads*), indicating the NT cleavage event in Fig. 1*A* is not a result of the SNAP tag. Next, a FLAG-epitope tag was embedded into the SNAP-ADRA1D C terminus (SNAP-ADRA1D-CT-FLAG, 81.2 kDa) between residues Glu^{473} and Pro^{474} using inFusion cloning technology. Immunoblotting anti-FLAG immunoprecipitated HEK293T cell lysates transfected with SNAP-ADRA1D-CT-FLAG revealed bright oligomeric, dimeric, and monomeric species, as well as a faint band at ~75 kDa equal in size to the ADRA1D minus the NT (Fig. 1*D*). In contrast, a β1-AR (ADRB1) chimera containing the ADRA1D NT (amino acids 1–98 of ADRA1D fused to amino acids 61–477 of ADRB1, 73.6 kDa) did not produce the cleavage band (Fig. 1*E*), suggesting the ADRA1D NT is not sufficient to ensure this event occurs, but rather that the transmembrane domains, loops, and/or C terminus are required.

Remarkably, transfecting SNAP-ADRA1D into human cell lines of varying tissue origin produced nearly identical protein band patterns (Fig. 2). These data infer that the ADRA1D NT is endogenously cleaved in human cells.

ADRA1D NT Is Cleaved between Leu^{90} and Val^{91}—Our next objective was to identify the location of the processing site on the ADRA1D NT. SNAP-ADRA1D NT truncation mutants were subcloned with inFusion technology, transfected into HEK293T cells, and imaged with LI-COR Odyssey. Δ1–58 and Δ1–79 ADRA1D constructs were included as these mutants were the prototypes first demonstrated to facilitate ADRA1D functional responses *in vitro* (25–27). ADRA1D NT deletions with four amino acid increments spanning 79 to 95 were cloned. As shown, NT truncation bands were detected for WT, Δ1–58, Δ1–79, Δ1–83, and Δ1–87 species but not Δ1–91 nor Δ1–95 (Fig. 3*A*). We thus proceeded to truncate individual amino acids between 87 and 91. ADRA1D NT bands were observed with each successive amino acid truncation, until Δ1–91, which displayed no NT band, indicating this is the location where ADRA1D NT cleavage occurs (Fig. 3*B*; supplemental Fig. S1 demonstrates equal protein loading was achieved as assessed by anti-GAPDH Western blotting and that transfection efficiencies are consistent across samples).

Δ1–91 ADRA1D Demonstrates Enhanced Agonist-stimulated Dynamic Mass Redistribution Responses—The data generated thus far insinuate that ADRA1D exists as two entities in human cells, full-length and Δ1–91 ADRA1D. However, the functional implications of this proteolytic processing event remain unclear. We previously discovered the ADRA1D exists as a modular homodimer, with one ADRA1D protomer bound to the PDZ protein syntrophin and the dystrophin-associated protein complex, and the second ADRA1D promoter bound to the multi-PDZ domain scaffold scribble (32). Thus, we hypothesized NT cleavage represents a mandatory processing checkpoint during assembly of ADRA1D macromolecular complexes. Moreover, we postulated that the signaling complex assembly occurs during ER/Golgi transport and that the ADRA1D NT acts as a recognition domain to ensure proper protein-protein docking and trafficking. If this postulate were correct, we would expect Δ1–91 ADRA1D would be unable to associate with known PDZ-protein binding partners. This was not the case. Rather, co-immunoprecipitation/immunoblotting (Fig. 3*C*) demonstrated TAP-syntrophin (*3rd lane*) and TAP-scribble (*4th lane*) interacted with multimeric and homodimerized NT FLAG-tagged Δ1–91 ADRA1D (denoted by *arrow*, 106.2 kDa, or 53.1 per monomer). To validate this result, we employed TAP LC-MS/MS analyses (Table 1 and supplemental Table S1) using TAP-Δ1–91 ADRA1D as bait protein in HEK293T cells. Scribble, syntrophins, and dystro-

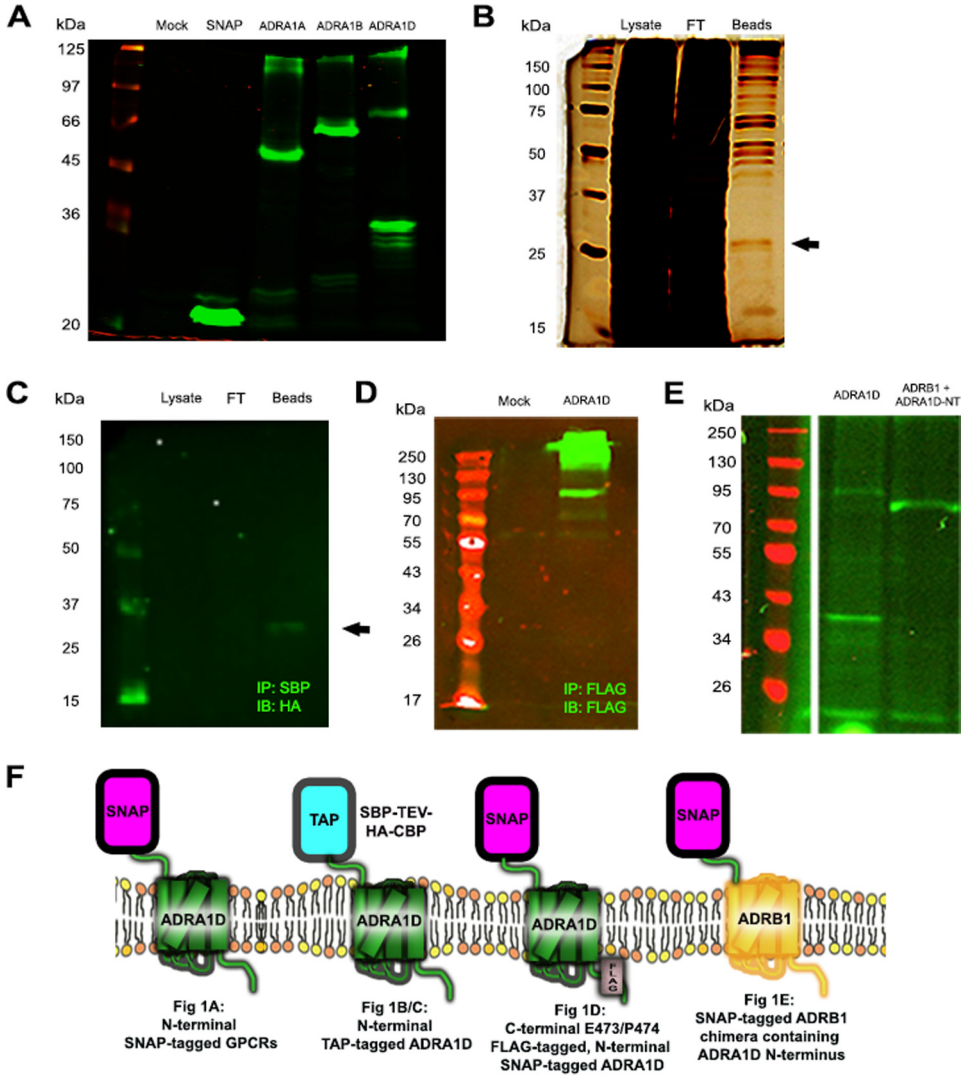

FIGURE 1. **ADRA1D N-terminal domain is cleaved in cultured human cells.** *A*, LI-COR imaging of N-terminal SNAP-α_1-AR subtypes in HEK293T lysates. α_{1A} (ADRA1A) and α_{1B} (ADRA1B) subtypes are observed as primarily full-length species and dimers/oligomers. Full-length α_{1D}-AR (ADRA1D) is detected (80.3-kDa band), as well as a smaller band ~30 kDa in size. *B* and *C*, ADRA1D N-terminal cleavage bands (denoted with *arrow* on *right side*) are detected with silver stain (*B*) and anti-HA immunoblotting (*C*) following streptavidin-binding protein affinity purification of N-terminal TAP-ADRA1D (72.2 kDa) from digitonin-solubilized HEK293T lysates. *D*, SNAP-ADRA1D containing a C-terminal FLAG-epitope tag embedded between Glu^{473} and Pro^{474} was immunoprecipitated (*IP*)/immunoblotted (*IB*) from HEK293T lysates. Most ADRA1D is detected as oligomers/dimers. Faint full-length (81.2 kDa) and truncated (~75 kDa) ADRA1D bands are detectable. *E*, chimeric β1-AR (ADRB1) containing the SNAP-ADRA1D N terminus (73.6 kDa) does not undergo N-terminal processing in HEK293T cells. *F*, schematic of epitope-tagged GPCRs used. *SBP*, streptavidin-binding protein; *TEV*, tobacco etch virus cleavage site; *HA*, hemagglutinin; *CBP*, calmodulin-binding protein.

phin-associated complex members (UTRN, utrophin; CTNNAL1, α-catulin, DTNA, α-dystrobrevin, and DMD, dystrophin) were identified in TAP-Δ1–91 ADRA1D proteomic screens, as well as TAP-Δ1–90 and TAP-Δ1–79 ADRA1D, indicating NT cleavage does not affect interactions with PDZ proteins.

As an alternative, we tested the notion that ADRA1D NT truncation may impact agonist efficacy. This was evaluated by comparing label-free dynamic mass redistribution (DMR) responses for the α_1-AR agonist phenylephrine at WT and Δ1–91 ADRA1D in HEK293T cells (Fig. 4, *A–E*) using the method established in previous DMR studies (33, 34). As a control, the prototype NT ADRA1D mutant, Δ1–79 ADRA1D, was included in the experimental protocol (Fig. 4*B*) to facilitate cross-analysis with previous ADRA1D NT studies (25–27). α_1-AR agonist efficacies are typically in the rank order of ADRA1A ⋙ ADRA1B > ADRA1D in cell culture assays (35). Consequently ADRA1A was also assayed and used as a benchmark for maximal intrinsic activity (Fig. 4*E*). Phenylephrine concentration-response curves were calculated using the time point at which peak DMR values were observed (Fig. 4*F*).

As expected, phenylephrine-stimulated ADRA1D responses (Fig. 4, *A* and *F*; Table 2) are of lower intrinsic activity (IA = 0.31) and potency (EC_{50} = 9.47 μM) relative to ADRA1A (IA = 1; EC_{50} = 0.57 μM) (Fig. 4*E* and supplemental Fig. S2 and supplemental Table S2). Interestingly, Δ1–91 ADRA1D phenylephrine responses (Fig. 4, *C* and *F*; IA = 0.4; EC_{50} = 4.3 μM) were significantly greater than WT ADRA1D, but less potent than Δ1–79 ADRA1D (Fig. 4, *B* and *F*; IA = 0.38; EC_{50} = 0.094 μM). Truncation of the C-terminal PDZ ligand abrogated Δ1–91 ADRA1D responses (Fig. 4, *D* and *F*), which also occurs when

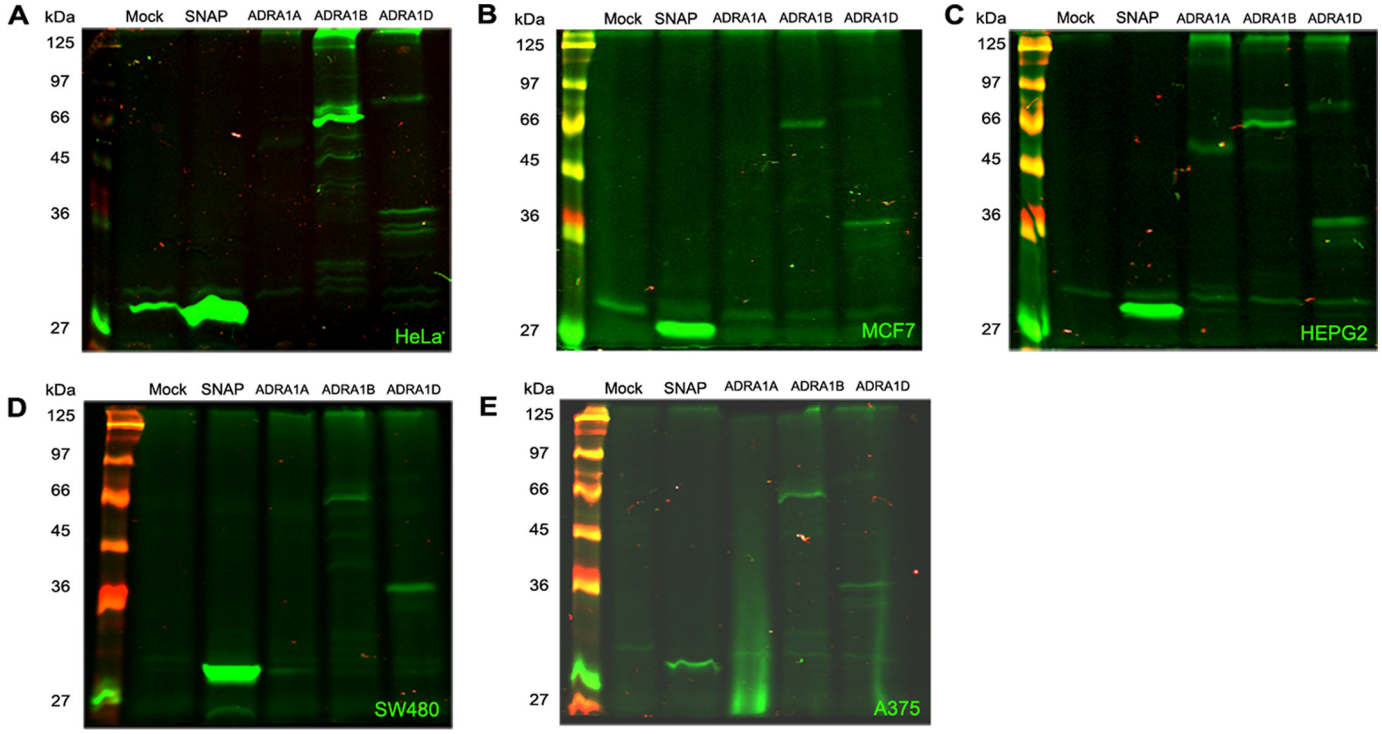

FIGURE 2. **ADRA1D N-terminal processing occurs in multiple human cell lines of diverging tissue origin.** SNAP-α_{1D} (ADRA1D) full-length and N-terminal protein bands were detectable via LI-COR near-infrared imaging in the following: *A*, HeLa (cervix); *B*, MCF-7 (breast); *C*, HEPG2 (liver); *D*, SW480 (colon); and *E*, A375 (skin) immortalized cell lines.

removing the PDZ ligand from Δ1–79 ADRA1D (28). Thus, the Δ1–91 ADRA1D species displays enhanced agonist efficacy relative to the unprocessed receptor and requires an intact PDZ ligand to impart full function.

Sterically Blocking ADRA1D NT Cleavage Diminishes Agonist Efficacy—Our DMR data suggest ADRA1D NT truncation enhances agonist efficacy and that cells employ this molecular tactic to regulate ADRA1D function. If true, inhibiting ADRA1D NT cleavage should diminish agonist efficacy, as all the ADRA1D species in a cell would be full-length, rather than a mixture of full-length and Δ1–91 ADRA1D. Thus, we sought methods to block NT ADRA1D processing. We first queried the ADRA1D NT peptide for predicted protease cleavage sites (www.expasy.org). These included the following: Arg-C proteinase (ADRA1D NT amino acids 4, 15, and 66); Asp-N endopeptidase (amino acids 4, 16, 63, and 79); chymotrypsin (amino acids 3 and 11); clostripain (amino acids 4, 15, and 66); formic acid (amino acids 5, 17, 64, and 80); glutamyl peptidase (amino acids 12, 39, 63, and 71); pepsin (amino acids 2, 3, 5, 7, 10, 11, 89, and 90); proteinase K (>20 sites identified); thermolysin (>20 sites identified); and trypsin (amino acids 4 and 66). Despite the vast number of predicted protease cleavage sites, a broad range protease inhibitor mixture (PIC) containing aprotinin, bestatin, E-64, leupeptin, and pepstatin A had no observable effect on the SNAP-ADRA1D NT peptide pattern (Fig. 5*A*). We also identified a putative matrix metalloproteinase cleavage site at ^{89}GL^{90}, yet the matrix metalloproteinase inhibitor doxycycline also demonstrated no discernable effects (Fig. 5*B*) nor did the proteasome inhibitor MG132, suggesting ADRA1D NT cleavage is not a result of non-specific protein degradation (Fig. 5*C*). The ER/Golgi transport inhibitor brefeldin A also had no effect, which led us to speculate that the ADRA1D NT processing occurs before the receptor reaches the plasma membrane (Fig. 5*D*). Moreover, incubating cells with α_1-AR agonist phenylephrine (*PHE,* Fig. 5*E*) or α_1-AR antagonist prazosin (*PRZ,* Fig. 5*F*) did not alter ADRA1D NT cleavage, indicating this processing event is independent of ADRA1D activation state.

In light of our failed attempts to block ADRA1D NT processing pharmacologically, we turned to a structural approach. Molecular modeling suggested replacing ^{89}GLVVSAQ^{95} with amino acids containing bulky, chemically dissimilar R-groups may introduce steric hindrance, thereby preventing proteases from accessing the ^{90}LV^{91} cleavage site. Insertion of a single Gly^{89}→ Pro^{89} point mutation had no effect on ADRA1D NT processing (Fig. 5*G*, *6th lane*). However, both triple S93P/A94P/Q95P (Fig. 5*G*, *4th lane*) and quintuple V91E/V92E/S93P/A94P/Q95P (Fig. 5*G*, *lane 5*) mutations lead to significant alterations in the ADRA1D NT peptide phenotype, as demonstrated by a reduction in SNAP-gel NT band density (^{93}PPP^{95} = 89.2% decrease; ^{91}EEPPP^{95} = 85.1% decrease in NT band intensity relative to WT ADRA1D).

ADRA1D NT mutants were then subjected to label-free DMR assays to assess the effect of inhibiting the NT cleavage event on agonist efficacy (Fig. 5*H*). Phenylephrine responses for the G89P ADRA1D mutant were equivalent to WT ADRA1D (IA = 0.39; EC_{50} = 10.6 μM), whereas ^{93}PPP^{95} (IA = 0.11; EC_{50} = 11.2 μM) and ^{91}EEPPP^{95} (IA = 0.17; EC_{50} = 7.7 μM) mutants displayed diminished phenylephrine intrinsic activities. To ensure observed DMR responses were consistent with previous studies that used reductionist $G\alpha_{q/11}$ signaling outputs to quantify ADR1D NT effects on agonist efficacy (25–27), we

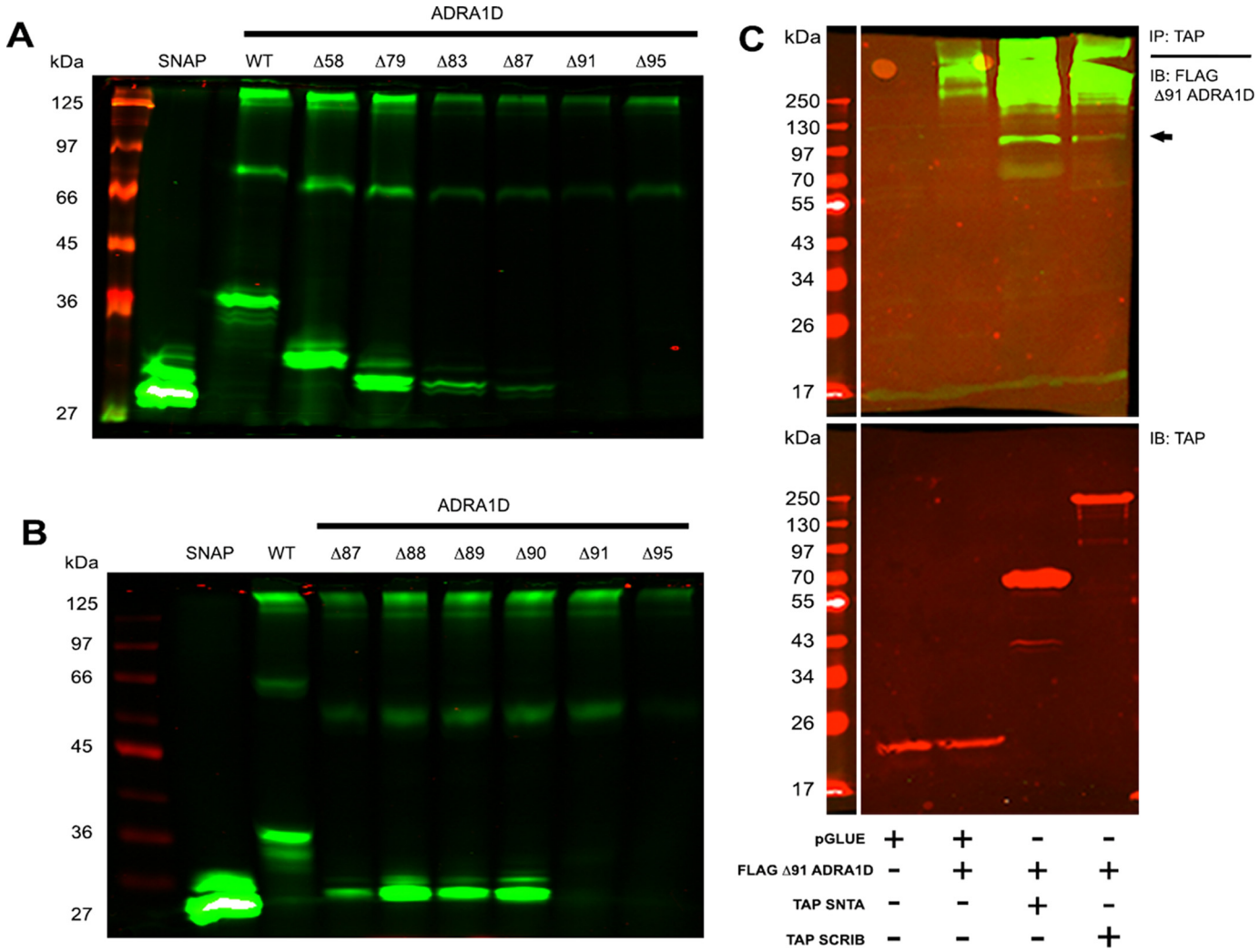

FIGURE 3. **ADRA1D N-terminal domain is cleaved between Leu^{90} and Val^{91}, producing an N-truncated ADRA1D that retains PDZ protein interactivity.** Sequential truncation analysis of SNAP-α_{1D} (ADRA1D) in HEK293T cell lysates was monitored by LI-COR near-infrared imaging. *A*, broad mapping indicates the ADRA1D N terminus is cleaved between and Gly^{87} and Val^{91}. *B*, single amino acid mapping pinpoints the cleavage site to be Leu^{90}/Val^{91}. Equal protein loading levels were confirmed with anti-GAPDH immunoblotting (*IB*) of transferred SNAP gels as shown in supplemental Fig. S1. *C*, Δ1–91-ADRA1D interacts with PDZ proteins. TAP α-syntrophin (*SNTA*, *3rd lane*) and TAP scribble (*SCRIB*, *4th lane*) co-immunoprecipitate (*IP*) robustly with multimeric/homodimeric FLAG Δ1–91 ADRA1D (106.2 kDa homodimers indicated by *arrow*) in HEK293T cells.

TABLE 1

TAP-MS/MS proteomic analysis of α_{1D}-AR (ADRA1D) truncation mutants

Data shown include percent peptide coverage (% Cov.), number of unique peptides (#UP), and PDZ and non-PDZ proteins detected. The following abbreviations are used: SCRIB = scribble; SNTA1 = α-syntrophin; SNTAB1 = β1-syntrophin; SNTAB2 = β2-syntrophin; CTNNAL1 = α-catulin; DMD = dystrophin; DTNA = dystrobrevin A; UTRN = utrophin. *** indicates protein not detected.

	ADRA1D		PDZ proteins			Non-PDZ proteins		
Clone ADRA1D	% Cov.	#UP	Name	% Cov.	#UP	Name	% Cov.	#UP
Δ1–79	19.2	8	SCRIB	2.8	4	CTNNAL1	6	2
			SNTA1	9.1	2	DMD	21	11
			SNTB1	43.1	16	DTNA	20	12
			SNTB2	59.1	27	UTRN	14.7	35
Δ1–90	3	4	SCRIB	1.9	3	CTNNAL1	3.5	2
			SNTA1	3.3	2	DMD	3.4	7
			SNTB1	19.6	5	DTNA	11.7	6
			SNTB2	17.8	11	UTRN	10.1	30
Δ1–91	2.6	2	SCRIB	1.9	3		***	***
				***	***	DMD	10.9	6
			SNTB1	10.5	3	DTNA	17.6	6
			SNTB2	15	8	UTRN	8.6	26

compared the ability of ADRA1D NT mutants to couple to phosphoinositol hydrolysis. HEK293T cells expressing individual ADRA1D constructs were stimulated with 100 μM phenylephrine for 1 h, and [^{3}H]inositol phosphates were quantified via ion exchange chromatography. Similar to our DMR datasets, the rank order of maximal responses for inositol phosphate production were Δ1–79 > Δ1–91 > WT > ^{91}EEPPP^{95} (Fig. 5*I*). Taken together, these functional experiments infer that full-length NT-intact ADRA1D responds sub-maximally to agonist stimulation and that NT truncation is necessary to produce optimally functional ADRA1D *in vitro*.

We queried this theory by quantifying WT, Δ1–91, and ^{91}EEPPP^{95} ADRA1D DMR responses stimulated by a panel of partial α_1-adrenergic receptor agonists, including oxymetazoline, cirazoline, naphazoline, synephrine, methoxamine, A61603, and tetrahydrozoline (Fig. 6, *A–D*, and Table 2). As a positive control, agonist DMR responses were quantified for the ADRA1A subtype (supplemental Fig. S2 and supplemental Table S2),

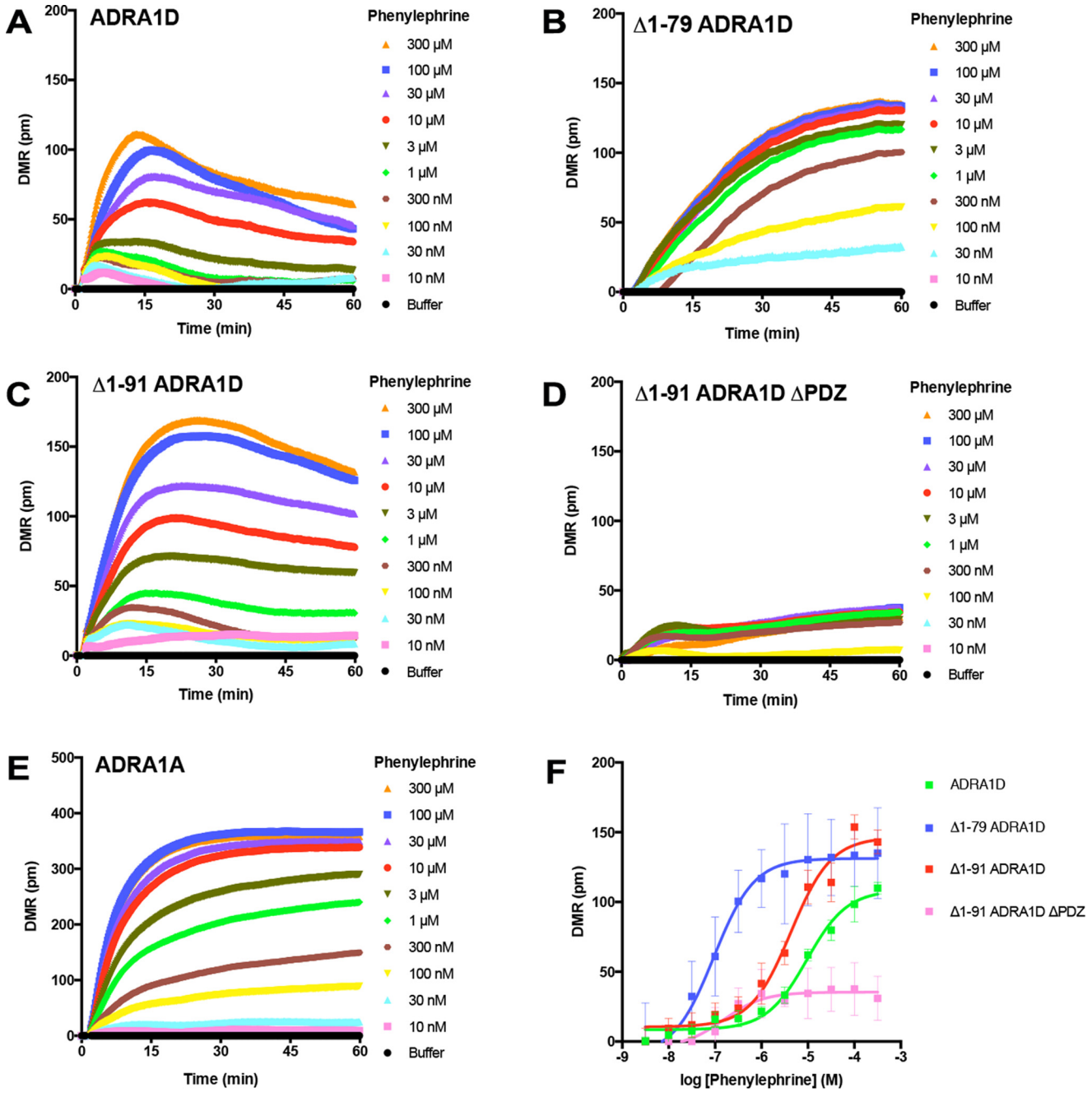

FIGURE 4. **Δ1–91 ADRA1D displays enhanced agonist efficacy in label-free DMR assays.** α_1-Adrenergic receptor agonist phenylephrine DMR responses were measured in HEK293T cells expressing SNAP. *A*, WT α_{1D} (ADRA1D); *B*, Δ1–79 ADRA1D; *C*, Δ1–91 ADRA1D; *D*, Δ1–91 ADRA1D ΔPDZ; or *E*, α_{1A} (ADRA1A). *F*, data were used to construct concentration-response curves to calculate phenylephrine potencies and intrinsic activities. Data are mean ± S.E. from 2 to 4 independent experiments performed with four replicates.

which is well documented to be the most functionally robust α_1-AR subtype in cell culture (10, 35).

As shown in Table 2, Δ1–91 ADRA1D maximal agonist-stimulated DMR responses were consistently greater than those observed for WT and ^{91}EEPPP^{95} ADRA1D. For example, Δ1–91 ADRA1D DMR responses stimulated by the partial agonist synephrine were 34% greater than those observed at WT ADRA1D and 46% greater than ^{91}EEPPP^{95}. Conversely, ^{91}EEPPP^{95} DMR maximal agonist responses were consistently equivalent (tetrahydrozoline, naphazoline, methoxamine, and A61603) or lower (phenylephrine, cirazoline, synephrine, and oxymetazoline) than those observed with WT ADRA1D. Thus, sterically hindering endogenous cleavage of the ADRA1D NT in human cells produces a full-length ADRA1D species with ameliorated agonist responsiveness.

We next examined whether ADRA1D NT truncation alters the typically intracellular sequestering of ADRA1D in a manner that facilitates its effective trafficking to the plasma membrane. This was queried first with SNAP-cell surface expression assays performed on intact HEK293T cells expressing individual ADRA1D NT species (Fig. 7*A*). Live HEK293T cells expressing NT-SNAP ADRA1D constructs were treated with the cell-im-

TABLE 2

Pharmacological properties of agonists targeting ADRA1D N-terminal mutants

Agonist-stimulated DMR concentration-response curves were constructed for wild type (WT), Δ1–91 truncated, and ^{91}EEPPP^{95} α_{1D} (ADRA1D) adrenergic receptors. Log molar agonist potencies (pEC_{50}) were calculated using the time at which peak DMR response (Max) was observed. All data were analyzed with GraphPad Prism and are expressed as mean ± S.E. of 3–4 independent experiments performed with four replicates. N-terminal mutant ADRA1D Max DMR values significantly different than WT ADRA1D Max DMR values are denoted with ** and potencies (pEC_{50} values) with ^^ (Student's *t* test, $p < 0.05$).

Agonist	ADRA1D					
	WT		Δ1–91		^{91}EEPPP^{95}	
	pEC_{50}	Max	pEC_{50}	Max	pEC_{50}	Max
		pm		*pm*		*pm*
Phenylephrine	−5.02 ± 0.10	109.92 ± 4.21	−5.14 ± 0.16	143.06 ± 4.48**	−5.11 ± 0.18	63.81 ± 6.63**
Cirazoline	−5.05 ± 0.12	77.19 ± 3.85	−6.67 ± 0.32^^	88.53 ± 5.78**	−5.80 ± 0.14^^	50.97 ± 2.54**
A61603	−5.24 ± 0.17	57.54 ± 4.10	−4.91 ± 0.17	96.30 ± 11.82**	−6.36 ± 0.26^^	51.48 ± 4.07
Naphazoline	−6.76 ± 0.21	48.20 ± 3.62	−6.10 ± 0.15^^	87.18 ± 10.73**	−6.88 ± 0.14	52.31 ± 7.52
Synephrine	−3.93 ± 0.09	72.62 ± 1.05	−4.39 ± 0.09^^	109.53 ± 2.60**	−4.62 ± 0.30^^	58.78 ± 4.38**
Tetrahydrozoline	−6.31 ± 0.38	26.52 ± 4.61	−6.16 ± 0.20	35.15 ± 0.67	−4.05 ± 0.25	31.45 ± 9.20
Methoxamine	−4.23 ± 0.41	29.41 ± 8.13	−4.30 ± 0.11	60.61 ± 2.81**	−4.50 ± 0.23	36.67 ± 7.10
Oxymetazoline	−4.64 ± 0.26	70.38 ± 4.01	−5.49 ± 0.24^^	95.92 ± 10.31**	−4.70 ± 0.51	37.15 ± 2.57**

permeable SNAP substrate BG 782 and quantified with LI-COR imaging. As shown, Δ1–91 ADRA1D cell surface expression is significantly greater than WT ADRA1D and ^{91}EEPPP^{95}, which correlates with the observed differences in DMR maximal responses (Fig. 4). Furthermore, [^{3}H]prazosin radioligand binding assays reveal Δ1–91 ADRA1D receptor density (B_{max} = 54.13 ± 8.14 fmol/mg protein) was greater than both WT (B_{max} = 32.48 ± 5.77 fmol/mg protein) and ^{91}EEPPP^{95} ADRA1D (B_{max} = 29.87 ± 6.58 fmol/mg protein) species in HEK293T cells (Fig. 7*B*). These B_{max} values are similar to α_1-AR B_{max} levels found in mouse liver and lung (36) and are thus expressed at physiologically relevant levels. These results were subsequently validated with live SNAP staining confocal imaging analyses (Fig. 7*C*). WT ADRA1D displayed plasma membrane expression in 26% of HEK293T cells, whereas Δ1–91 ADRA1D was observed at the plasma membrane in 65% of cells, as assessed by ImageJ analysis (supplemental Fig. S3). Thus, this study identifies endogenous NT cleavage as a mechanism to liberate ADRA1D from retention in the ER and permit plasma membrane expression, thereby facilitating efficient coupling to downstream signaling cascades.

Discussion

The importance of the NT for GPCR function has emerged as a subfield of intense study. With each successive report, it becomes increasingly evident that GPCRs can be categorized by the functional role of their NT domains. For example, certain GPCRs require obligate NT autoprocessing to become active. Members of the proteinase-activated receptor family undergo targeted proteolysis by various proteases (*i.e.* thrombin and trypsin) to unmask a "cryptic-tethered ligand" in the NT, which subsequently binds and activates the remainder of the intrinsic activity receptor transmembrane body (37). Adhesion GPCR NT domains contain conserved autoproteolysis sites (termed GPCR proteolytic site or GPCR-autoproteolysis-inducing) (38, 39). Uniquely, the adhesion GPCR, GPR56, undergoes obligate NT cleavage during ER/Golgi trafficking, creating a constitutively active receptor species that is modulated by binding of the NT (40). Our data demonstrating that the ADRA1D NT domain is not cleaved when fused to a chimeric β1-AR (ADRB1) suggests this domain does not undergo autoproteolysis. Rather, it infers the ADRA1D NT is cleaved by an as yet unidentified ubiquitously expressed protease that recognizes the ADRA1D transmembrane and/or loop domains to ensure specificity.

Alternatively, some GPCRs contain N termini that augment the binding properties of endogenous ligands. Prototypical examples are the metabotropic glutamate receptors, which use their extremely long NT to form the glutamate-binding site and modulate ligand selectivity (41). A double mutant polymorphism (R6G/E42G) in the 5HT2B serotonin receptor NT identified in drug-abuse patients (42) was found to negatively modulate both basal and agonist-stimulated receptor activity (43). A similar mechanism has been demonstrated for the H1 histamine receptor, where NT domain association with extracellular loop 2 imparts distinct pharmacological properties to the receptor (44). Additionally, NT polymorphisms in β-adrenergic receptors affect the duration of agonist activity by controlling receptor desensitization and internalization rates (45, 46). Label-free DMR signaling assays suggest ADRA1D NT cleavage alters agonist efficacy, as measured by potency and intrinsic activity. However, SNAP cell surface and confocal imaging assays indicate this is a result of enhanced ADRA1D plasma membrane expression, rather than a structural effect exerted by the NT on the transmembrane domains or intracellular loops to regulate signal transduction coupling. In some cases, ligands can differentially regulate NT processing, such as the β1-AR, which undergoes enhanced NT cleavage when treated with agonists, and minimal NT cleavage with antagonists (47, 48). Although no effects of the α_1-AR antagonist prazosin or the α_1-AR agonist phenylephrine on ADRA1D NT processing were observed, it is possible that other α_1-AR ligands may differentially regulate this cellular event via ligand-biased signaling mechanisms.

GPCR NT domains can also facilitate proper assembly and impart stability to GPCR macromolecular complexes. In a seminal study, FRET analysis demonstrated the NT of the *Saccharomyces cerevisiae* STE2 α-factor GPCR contributes to the stable formation of receptor oligomers, together with transmembrane domains 1 and 2 (49). This feature is shared by several receptors, including mGluR1 metabotropic glutamate (41), Ca^{2+}-sensing (50), and $GABA_B$ R1/R2 receptors (51). In our study, however, truncation of the proximal

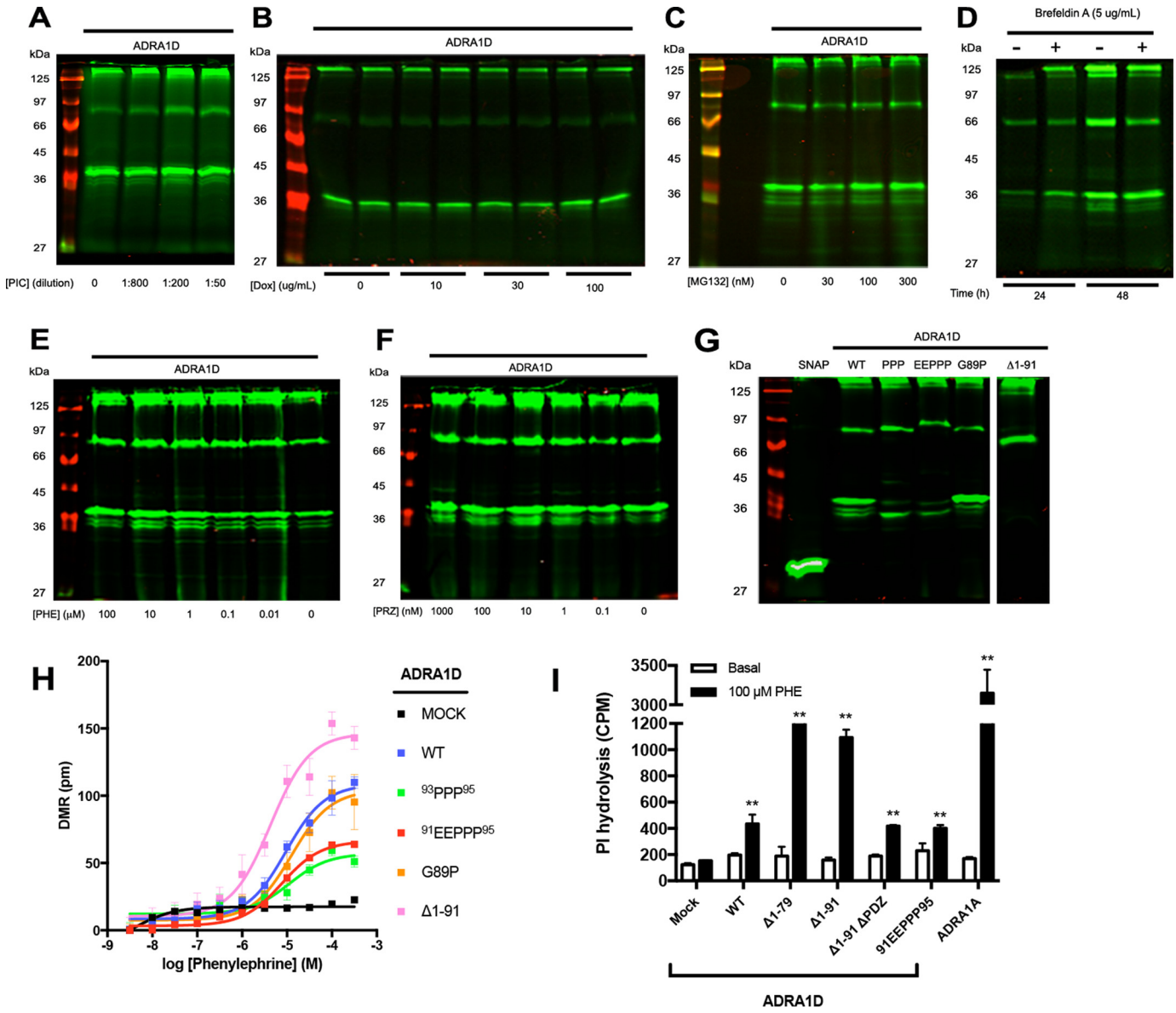

FIGURE 5. **Steric hindrance alters ADRA1D N-terminal processing and diminishes agonist-stimulated DMR responses.** LI-COR imaging of SNAP-α_{1D} (ADRA1D) was used to assess the ability of various pharmacological agents to affect N-terminal processing, including the following: *A*, protease inhibitor mixture (*PIC*) containing aprotinin, bestatin, E-64, leupeptin, and pepstatin A; *B*, matrix metalloproteinase inhibitor doxycycline; *C*, proteasome inhibitor MG132; *D*, ER/Golgi-transport inhibitor brefeldin A; *E*, α_1-adrenergic receptor agonist phenylephrine (*PHE*); or *F*, α_1-adrenergic receptor antagonist prazosin (*PRZ*). *G*, targeted mutations ^{93}PPP^{95}, ^{91}EEPPP^{95}, or ^{G}89^{P} were inserted into the SNAP-ADRA1D to add steric hindrance to the putative ADRA1D N-terminal cleavage site using inFusion mutagenesis and then examined with SNAP-PAGE LI-COR imaging. Changes in ADRA1D NT band intensity were quantified with Image Studio Lite (LI-COR) *H*, α_1-adrenergic receptor agonist phenylephrine DMR responses were measured in HEK293T cells expressing SNAP-WT, Δ1–91, ^{93}PPP^{95}, ^{91}EEPPP^{95}, or G89P ADRA1D. Data are mean ± S.E. from 3 to 4 independent experiments performed with four replicates. *I*, phosphoinositol (*PI*) hydrolysis levels were quantified following addition of 100 μM phenylephrine to untransfected (MOCK) or HEK293T cells expressing WT, Δ1–79, Δ1–91, ^{91}EEPPP^{95} ADRA1D, or ADRA1A. Data are mean ± S.E. from three independent experiments performed with three replicates. ** indicates increase in phosphoinositol hydrolysis with 100 μM phenylephrine was significantly greater than buffer as determined by unpaired *t* test ($p < 0.05$).

91-amino acid ADRA1D produced no detectable differences in higher order oligomer formation or PDZ protein interactions, as revealed by SNAP-gel imaging and TAP LC-MS/MS proteomic screens.

Instead, our data suggest the ADRA1D belongs to a small subset of GPCRs that require NT processing to ensure optimal function but do not appear to use the NT as a ligand nor require the NT to bind exogenous ligand. A prototype member of this group is the CB1 cannabinoid receptor, which contains a 116-amino acid NT domain that inhibits CB1 translocation and maturation in cultured cells, resulting in minimal plasma membrane receptor expression (52). Remarkably, the molecular and biochemical features of GPR37, or parkin-associated endothelin-like receptor, are uncannily similar to the ADRA1D. GPR37 also contains an unusually long NT domain that must be removed to facilitate functional expression at the plasma membrane, as well as a C-terminal PDZ ligand, which in this case interacts with PDZ-domain protein syntenin-1. Like syntrophins and scribble for the ADRA1D, the syntenin-1 interaction is necessary to achieve significant GPR37 plasma membrane expression (53). Thus, we propose ADRA1D and GPR37 are core members of a unique group of GPCRs that

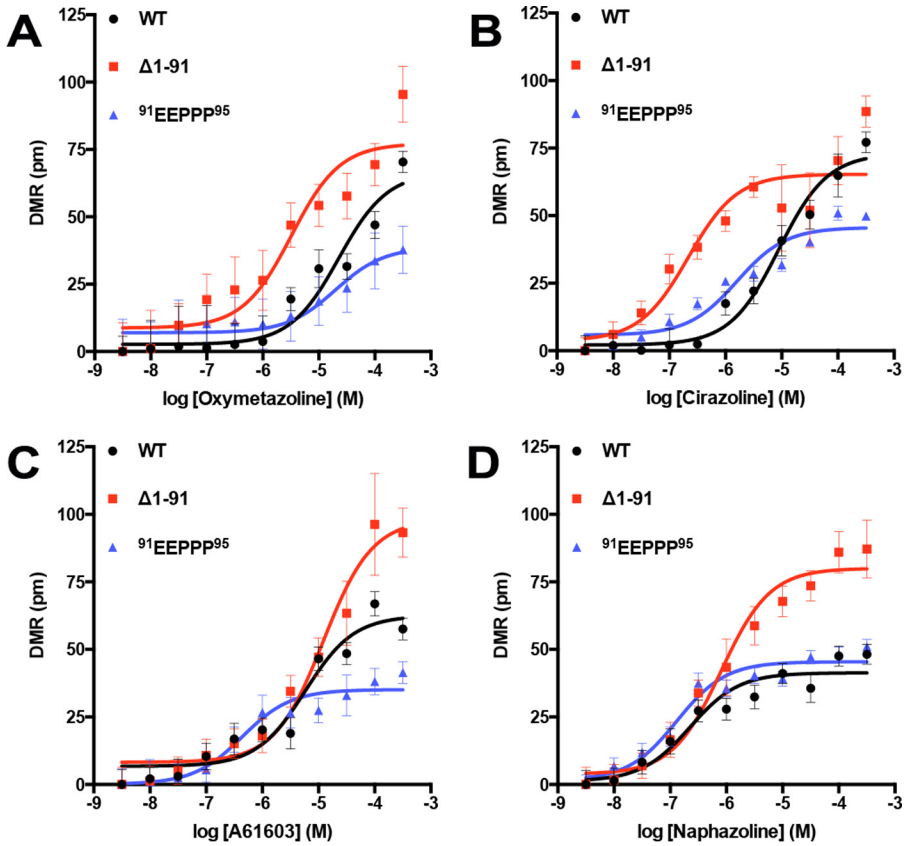

FIGURE 6. **^{91}EEPPP^{95} ADRA1D displays abrogated α_1-AR agonist efficacies.** SNAP-WT, Δ1–91, and ^{91}EEPPP^{95} α_{1D} (ADRA1D) DMR responses stimulated by α_1-adrenergic receptor agonists oxymetazoline (*A*), cirazoline (*B*), A61603 (*C*), or naphazoline (*D*) were quantified to calculate potency and intrinsic activity. Data are summarized in Table 2 and are the mean ± S.E. of three independent experiments performed with four replicates.

require obligate NT processing and PDZ protein interactions to sustain optimal function in human cells. Given that at least 55 GPCRs have been identified that contain putative PDZ ligands in their C termini (54), it is likely one or more of these PDZ GPCRs may display similar NT processing properties as ADRA1D and GPR37.

In summary, we and others have previously reported molecular truncation of the ADRA1D NT is a convenient albeit unexplained experimental strategy that rescues ADRA1D from endoplasmic reticulum sequestration. As a consequence, artificially truncated receptors accumulate at the plasma membrane that display enhanced agonist-stimulated responses (25–27). However, no compelling evidence existed indicating this event occurs in physiological contexts. Thus, our discovery that the ADRA1D NT domain is cleaved in cultured human cells was entirely unexpected. This observation was validated by multiple biochemical and pharmacological approaches and shown to occur in multiple cell lines of varying tissue origin. Most interestingly, the ability of a cell to process the ADRA1D NT directly correlates with agonist efficacy, representing an alternative mechanism cells use to regulate ADRA1D function during assembly/trafficking. With GPR37, the ADRA1D belongs to a unique group of GPCRs that undergo obligate NT processing and PDZ protein interactions to achieve plasma membrane expression. Thus, developing novel therapeutics aimed at selectively modulating cellular mechanisms that regulate GPCR-specific NT processing events represents a novel and potentially powerful path for GPCR drug discovery.

Experimental Procedures

Plasmids, Chemicals, and Antibodies—Human ADRA1D cDNAs were subcloned and mutated in pSNAPf (New England Biolabs) using In-Fusion HD cloning technology (Clontech). (*R*)-(−)-Phenylephrine hydrochloride (P6126), prazosin HCl (P7791), MG132 (M7449), brefeldin A (B7651), protease inhibitor mixture (P1860), and doxycycline HCl (D3447) were purchased from Sigma. SNAP-782 substrate was from New England Biolabs (S9142S). Alexa fluor 633 goat anti-rabbit IgG (A-21070) and Alexa fluor 568 goat anti-rat (A-11011) antibodies and Topro-3 iodide (T3605) were from Life Technologies, Inc. Rabbit polyclonal α-syntrophin (H-65, sc-50460), and rabbit polyclonal anti-scribble (H-300, sc-28737) antibodies from Santa Cruz Biotechnology. Mouse monoclonal anti-syntrophin (1351, ab11425) antibody and rabbit polyclonal anti-Myc tag antibody (ab9106) were from Abcam. Anti-HA mouse mAb (6E2, 2367) was from Cell Signaling. IRdye 680 goat anti-mouse IgG and IRdye 800cw goat anti-rabbit IgG were from LI-COR.

Cell Culture and Reagents—Human embryonic kidney (HEK) 293T, SW480, HEPG2, MCF7, and A375 cells were grown in Dulbecco's modified Eagle's medium (DMEM) supplemented with 10% fetal bovine serum and 2 mM L-glutamine. Cells were transfected with 1 mg/ml polyethyleneimine (PEI) and used 24–48 h post-transfection.

SNAP-PAGE—HEK293T cells were transfected with SNAP-tagged proteins. 48 h after transfection, cells were lysed with 50

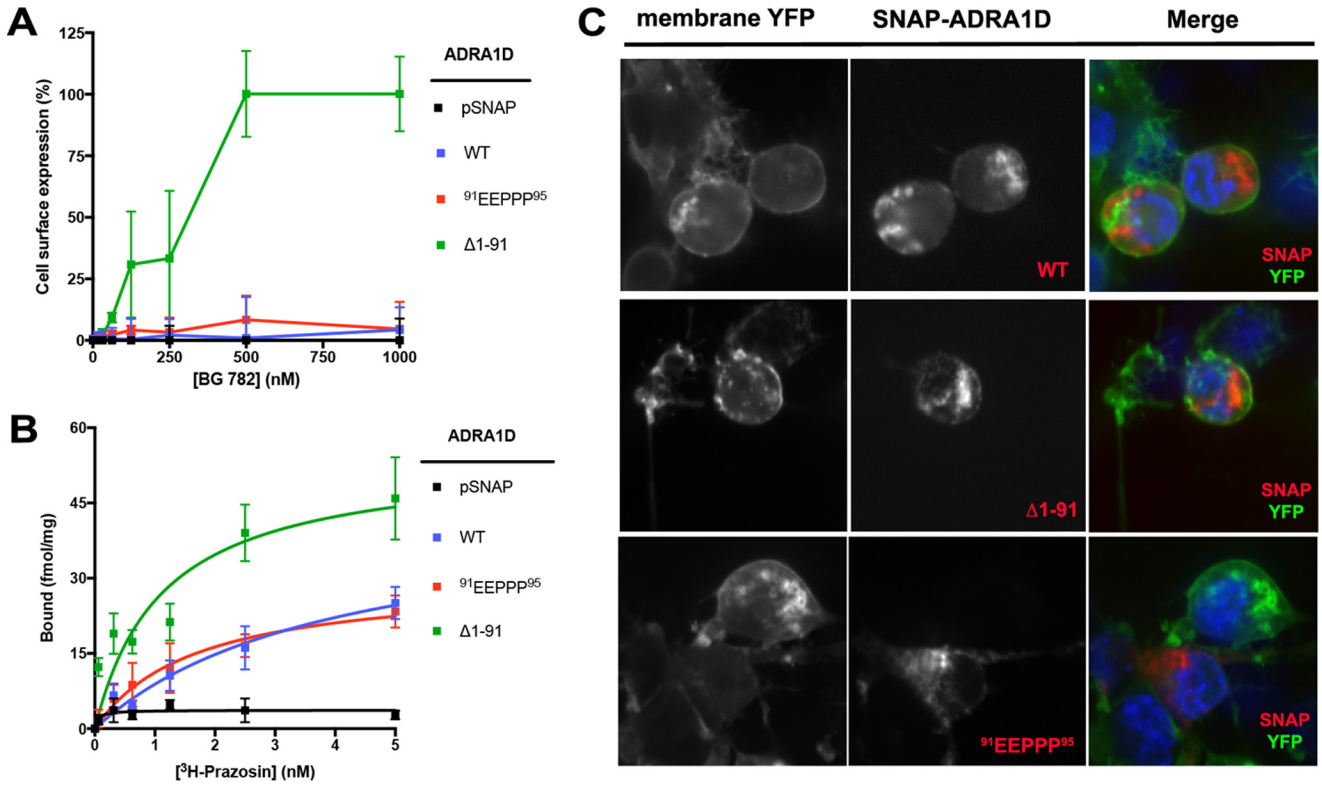

FIGURE 7. **N-terminal processing facilitates ADRA1D plasma membrane expression.** *A*, SNAP cell-surface expression was quantified for pSNAP vector, WT, and α_{1D} (ADRA1D) mutants ^{91}EEEPP^{95} and Δ1–91 in HEK293T cells. Data are mean ± S.E. of three independent experiments performed with three replicates. *B*, [^{3}H]prazosin radioligand saturation binding assays of HEK293T cell lysates expressing pSNAP vector, SNAP-WT, Δ1–91, or ^{91}EEEPP^{95} ADRA1D. Data are mean ± S.E. of 2–3 independent experiments performed with three replicates. *C*, SNAP live-cell confocal imaging analysis of WT, Δ1–91, and ^{91}EEEPP^{95} ADRA1D in HEK293T cells. SNAP-ADRA1D constructs were co-transfected with membrane YFP marker and are displayed alone (membrane YFP, *left column*; ADRA1D, *middle column*) or merged (*right column*) with SNAP-ADRA1D constructs in *red* and membrane YFP in *green*. DAPI stain to mark nuclei is shown in *blue*. Data were quantified with ImageJ as described in supplemental Fig. S3.

mM Tris-HCl, 150 mM NaCl, 1% Nonidet P-40, and 0.1% Tween 20 buffer. 0.5 μM BG-782 substrate and 1 mM DTT were added to lysates, and samples were incubated for 30 min at 37 °C in the dark. Samples were then run on SDS-PAGE, and gels were imaged using the LI-COR Odyssey Scanner.

Affinity Purification/Immunoblotting—Cells were harvested and lysed in 0.5% digitonin, 75 mM Tris (pH 8.0), 2 mM EDTA, 5 mM $MgCl_2$, 1 mM DTT with protease and phosphatase inhibitors. Cleared supernatants were then subjected to affinity purification with streptavidin-Sepharose (GE Healthcare) for 3 h at 4 °C. Streptavidin beads were washed four times with lysis buffer. Samples were denatured by boiling in 4× sample buffer at 90 °C for 10 min. Gels were transferred to nitrocellulose membrane and blocked for 1 h at room temperature and then probed with primary antibodies as indicated overnight at 4 °C. Primary antibodies were detected with IRDye 800CW goat anti-rabbit or IRDye 680 goat anti-mouse and imaged with LI-COR Odyssey Scanner (LI-COR Biotechnology).

TAP and LC-MS/MS Mass Spectrometry—TAP has been described previously (23). Eluates were directly analyzed on a Velos-Pro Orbitrap Elite hybrid mass spectrometer (Thermo Fisher). Raw MS data were searched with SEQUEST (Thermo Fisher) or COMET (55), and protein false discovery rate was set at 2.5%.

Label-free DMR Assays—DMR assays were performed using a method derived from previously documented studies (33, 34). HEK293T cells were seeded at ~500,000/well in Corning Epic sensor microplates and cultured for 24 h. Cells were washed three times with HBSS buffer and transferred to the Corning Epic BT reader, which was permanently housed in a Thermo cell culture incubator at 37 °C with 5% CO_2, as this magnified the amplitude of recorded DMR responses. Baseline DMR measurements were recorded for 1 h. Compounds were added with the Sorenson Biosciences 96-well Benchtop Pipettor, and agonist DMR responses were recorded for 1 h. Data were exported to Microsoft Excel using Epic Analyzer Software.

Phosphoinositol Hydrolysis Assay—HEK293T cells were transfected with SNAP-ADRA1D constructs and pre-labeled with 1 mCi/ml [^{3}H]myo-inositol (American Radiolabeled Chemicals Inc). After 48 h, cells were stimulated with 100 μM phenylephrine for 1 h in HBSS buffer + 10 mM LiCl. Total inositol phosphates were purified via Dowex ion exchange chromatography using the method described previously (26).

SNAP-cell Surface Expression—HEK293 cells were seeded in 6-well plates at 8×10^5 cells/well. Cells were transfected with SNAP-tagged cDNA constructs/PEI and replated in 96-well black optical bottom cell culture plates. SNAP-surface 782 substrate was diluted in DMEM to the designated concentrations and incubated at 37 °C, 5% CO_2 for 30 min. Cells were washed, fixed with 4% paraformaldehyde, and then incubated with 1:10,000 nuclear stain TOPRO-3 to normalize for cell number. Plates were analyzed with LI-COR Odyssey Scanner (LI-COR

Biotechnology), and signal intensity was quantified as mean cell surface expression ± S.E.

Radioligand Binding—[^{3}H]Prazosin saturation assays were performed as described previously (23, 26). Cell membranes were prepared from HEK293T cells, incubated with [^{3}H]prazosin for 30 min at 37 °C, subjected to Brandel vacuum filtration (Brandel, Gaithersburg, MD), and counted with a Tri-Carb 2200 CA liquid scintillation analyzer (Packard Instrument Co. Inc., Rockville, MD). Nonspecific binding was determined with 100 μM phentolamine. Data were analyzed with GraphPad Prism 6 software and expressed as mean ± S.E.

SNAP Live Cell Imaging—HEK293T cells were transfected with 250 ng of SNAP-tagged ADRA1D cDNA constructs in a glass bottom tissue culture dish (MatTek). After 48 h, cells were treated with 1 μM SNAP-cell 505-STAR (New England Biolabs) for 30 min, washed, and incubated in fresh media containing NucBlue DNA stain (Life Technologies, Inc.) for 30 min. Cells were washed and incubated in fresh fluorescence-compatible media (Fluorobrite, Gibco) supplemented with 10% FBS for 10 min. Images were acquired with a Yokogawa CSU10 spinning disk confocal mounted on a Leica DMI6000B with a ×63 objective lens. Quantification of membrane enrichment was performed with ImageJ. Plasma membranes were outlined based on membrane-targeted YFP localization, and the intracellular fluorescent signal was subtracted. For each individual cell, two discrete intracellular regions were quantified to represent a cytosolic signal. All values collected were normalized by area. Enrichment values were calculated as the ratio of signal per area of membrane to the signal per area of cytosol. Significance was calculated using Student's t test ($p < 0.001$).

Author Contributions—T. S. K., K. S. L., S. A.-H., N. D. C., A. W. Y., E. H. W., J. D. S., and C. H. designed the experiments. T. S. K., K. S. L., S. A.-H., E. C., J. M. P., D. A. H., A. S., J. H., N. D. C., and C. H. performed the experiments. T. S. K., N. D. C., E. H. W., J. D. S., and C. H. wrote the manuscript.

Acknowledgments—We thank Professor Ning Zheng (Howard Hughes Medical Institute, Department of Pharmacology, University of Washington) for help with structural analyses of the ADRA1D N-terminal domain.

References

1. García-Sáinz, J. A., and Villalobos-Molina, R. (2004) The elusive α_{1D}-adrenoceptor: molecular and cellular characteristics and integrative roles. *Eur. J. Pharmacol.* **500,** 113–120
2. Perez, D. M., Piascik, M. T., and Graham R. M. (1991) Solution-phase library screening for the identification of rare clones: isolation of an α_{1D}-adrenergic receptor cDNA. *Mol. Pharmacol.* **40,** 876–883
3. Piascik, M. T., Smith, M. S., Soltis, E. E., and Perez D. M. (1994) Identification of the mRNA for the novel α_{1D}-adrenoceptor and two other α_1-adrenoceptors in vascular smooth muscle. *Mol. Pharmacol.* **46,** 30–40
4. Piascik, M. T., Guarino, R. D., Smith, M. S., Soltis, E. E., Saussy, D. L., and Perez, D. M. (1995) The specific contribution of the novel α_{1D} adrenoceptor to the contraction of vascular smooth muscle. *J. Pharmacol. Exp. Ther.* **275,** 1583–1589
5. McCune, D. F., Edelmann, S. E., Olges, J. R., Post, G. R., Waldrop, B. A., Waugh, D. J., Perez, D. M., and Piascik M. T. (2000) Regulation of the cellular localization and signaling properties of the α_{1B}- and α_{1D}-adrenoceptors by agonists and inverse agonists. *Mol. Pharmacol.* **57,** 659–666
6. Chalothorn, D., McCune, D. F., Edelmann, S. E., García-Cazarín, M. L., Tsujimoto, G., and Piascik, M. T. (2002) Differences in the cellular localization and agonist-mediated internalization properties of the α_1-adrenoceptor subtypes. *Mol. Pharmacol.* **61,** 1008–1016
7. Hague, C., Uberti, M. A., Chen, Z., Hall, R. A., and Minneman, K. P. (2004) Cell surface expression of α_{1D}-adrenergic receptors is controlled by heterodimerization with α_{1B}-adrenergic receptors. *J. Biol. Chem.* **279,** 15541–15549
8. Uberti, M. A., Hague, C., Oller, H., Minneman K. P., and Hall, R. A. (2005) Heterodimerization with β2-adrenergic receptors promotes surface expression and functional activity of α_{1D}-adrenergic receptors. *J. Pharmacol. Exp. Ther.* **313,** 16–23
9. Hague, C., Lee, S. E., Chen, Z., Prinster, S. C., Hall, R. A., and Minneman K. P. (2006) Heterodimers of α_{1B}- and α_{1D}-adrenergic receptors form a single functional entity. *Mol. Pharmacol.* **69,** 45–55
10. Wang, S. Y., Song, Y., Xu, M., He, Q. H., Han, Q. D., and Zhang Y. Y. (2007) Internalization and distribution of three α_1-adrenoceptor subtypes in HEK293A cells before and after agonist stimulation. *Acta Pharmacol. Sin.* **28,** 359–366
11. García-Cazarín, M. L., Smith, J. L., Olszewski, K. A., McCune, D. F., Simmerman, L. A., Hadley, R. W., Kraner, S. D., and Piascik, M. T. (2008) The α_{1D}-adrenergic receptor is expressed intracellularly and coupled to increases in intracellular calcium and reactive oxygen species in human aortic smooth muscle cells. *J. Mol. Signal.* **3,** 6
12. Fan, L. L., Ren, S., Zhou, H., Wang, Y., Xu, P. X., He, J. Q., Luo, D. L. (2009) α_{1D}-Adrenergic receptor insensitivity is associated with alterations in its expression and distribution in cultured vascular myocytes. *Acta Pharmacol. Sin.* **30,** 1585–1593
13. Hampel, C., Dolber, P. C., Smith, M. P., Savic, S. L., Throff, J. W., Thor, K. B., and Schwinn, D. A. (2002) Modulation of bladder α_1-adrenergic receptor subtype expression by bladder outlet obstruction. *J. Urol.* **167,** 1513–1521
14. Bouchelouche, K., Andersen, L., Alvarez, S., Nordling, J., and Bouchelouche, P. (2005) Increased contractile response to phenylephrine in detrusor of patients with bladder outlet obstruction: effect of the α_{1A} and α_{1D}-adrenergic receptor antagonist tamsulosin. *J. Urol.* **173,** 657–661
15. Chen, Q., Takahashi, S., Zhong, S., Hosoda, C., Zheng, H. Y., Ogushi, T., Fujimura, T., Ohta, N., Tanoue, A., Tsujimoto, G., and Kitamura, T. (2005) Function of the lower urinary tract in mice lacking the α_{1D}-adrenergic receptor. *J. Urol.* **174,** 370–374
16. Walden, P. D., Gerardi, C., and Lepor, H. (1999) Localization and expression of the α_{1A}, α_{1B}-, and α_{1D}-adrenoceptors in hyperplastic and non-hyperplastic human prostate. *J. Urol.* **161,** 635–640
17. Kojima, Y., Sasaki, S., Kubota, Y., Imura, M., Oda, N., Kiniwa, M., Hayashi, Y., and Kohri, K. (2011) Up-regulation of α_{1A} and α_{1D}-adrenoceptors in the prostate by administration of subtype selective α_1-adrenoceptor antagonist tamsulosin in patients with benign prostatic hypertrophy. *J. Urol.* **186,** 1530–1536
18. Jensen, B. C., Swigart, P. M., Laden, M. E., DeMarco, T., Hoopes, C., and Simpson, P. C. (2009) The α_{1D} is the predominant α_1-adrenergic receptor subtype in human epicardial coronary arteries. *J. Am. Coll. Cardiol.* **54,** 1137–1145
19. Mishima, K., Tanoue, A., Tsuda, M., Hasebe, N., Fukue, Y., Egashira, N., Takano, Y., Kamiya, H. O., Tsujimoto, G., Iwasaki, K., and Fujiwara, M. (2004) Characteristics of behavioral abnormalities in α_{1D}-adrenoceptor deficient mice. *Behav. Brain Res.* **152,** 365–373
20. Aono, Y., Taguchi, H., Saigusa, T., Uchida, T., Takada, K., Takiguchi, H., Shirakawa, T., Shimizu, N., Koshikawa, N., and Cools A. R. (2015) Simultaneous activation of α_{1A}, α_{1B}, and α_{1D}-adrenoceptor subtypes in the nucleus accumbens reduces accumbal dopamine efflux in freely moving rats. *Behav. Pharmacol.* **26,** 73–80
21. Sadalge, A., Coughlin, L., Fu, H., Wang, B., Valladares, O., Valentino, R., and Blendy, J. A. (2003) α_{1D}-Adrenoceptor signaling is required for stimulus induced locomotor activity. *Mol. Psychiatry* **8,** 664–672
22. Tanoue, A., Koba, M., Miyawaki, S., Koshimizu, T. A., Hosoda, C., Oshikawa, S., and Tsujimoto, G. (2002) Role of the α_{1D}-adrenergic receptor in the development of salt-induced hypertension. *Hypertension* **40,** 101–106

23. Lyssand, J. S., DeFino, M. C., Tang, X. B., Hertz, A. L., Feller, D. B., Wacker, J. L., Adams, M. E., and Hague, C. (2008) Blood pressure is regulated by an α_{1D}-adrenergic receptor/dystrophin signalosome. *J. Biol. Chem.* **283,** 18792–18800
24. Morelli, M. B., Amantini, C., Nabissi, M., Liberati, S., Cardinali, C., Farfariello, V., Tomassoni, D., Quaglia, W., Piergentili, A., Bonifazi, A., Del Bello, F., Santoni, M., Mammana, G., Servi, L., Filosa, A., Gismondi, A., and Santoni, G. (2014) Cross-talk between α_{1D}-adrenoceptors and transient receptor potential vanilloid type 1 triggers prostate cancer cell proliferation. *BMC Cancer* **14,** 192
25. Pupo, A. S., Uberti, M. A., and Minneman, K. P. (2003) N-terminal truncation of human α_{1D}-adrenoceptors increases expression of binding sites but not protein. *Eur. J. Pharmacol.* **462,** 1–8
26. Hague, C., Chen, Z., Pupo, A. S., Schulte, N. A., Toews, M. L., and Minneman, K. P. (2004) The N terminus of the human α_{1D}-adrenergic receptor prevents cell surface expression. *J. Pharmacol. Exp. Ther.* **309,** 388–397
27. Petrovska, R., Kapa, I., Klovins, J., Schiöth, H. B., and Uhlén, S. (2005) Addition of a signal peptide to the α_{1D}-adrenoceptor gene increases the density of receptors, as determined by [^{3}H]prazosin binding in the membranes. *Br. J. Pharmacol.* **144,** 651–659
28. Chen, Z., Hague, C., Hall, R. A., and Minneman, K. P. (2006) Syntrophins regulate α_{1D}-adrenergic receptors through a PDZ domain-mediated interaction. *J. Biol. Chem.* **281,** 12414–12420
29. Lyssand, J. S., Whiting, J. L., Lee, K. S., Kastl, R., Wacker, J. L., Bruchas, M. R., Miyatake, M., Langeberg, L. K., Chavkin, C., Scott, J. D., Gardner, R. G., Adams, M. E., and Hague, C. (2010) α-Dystrobrevin-1 recruits α-catulin to the α_{1D}-AR/DAPC signalosome. *Proc. Natl. Acad. Sci. U.S.A.* **107,** 21854–21859
30. Jensen, B. C., Swigart, P. M., and Simpson, P. C. (2009) Ten commercial antibodies for α_1-adrenergic receptor subtypes are non-specific. *Naunyn. Schmiedebergs Arch. Pharmacol.* **379,** 409–412
31. Gong, H., Kovar, J. L., Baker, B., Zhang, A., Cheung, L., Draney, D. R., Corrêa, I. R., Jr., Xu, M. Q., and Olive, D. M. (2012) Near-infrared fluorescence imaging of mammalian cells and xenograft tumors with SNAP-tag. *PLoS ONE* **7,** e34003
32. Camp, N. D., Lee, K. S., Wacker-Mhyre, J. L., Kountz, T. S., Park, J. M., Harris, D. A., Estrada, M., Stewart, A., Wolf-Yadlin, A., and Hague, C. (2015) Individual protomers of a G protein-coupled receptor dimer integrate distinct functional modules. *Cell Discov.* **1,** 15011
33. Fang, Y., Ferrie, A. M., Fontaine, N. H., Mauro, J., and Balakrishnan, J. (2006) Resonant waveguide grating biosensor for living cell sensing. *Biophys. J.* **91,** 1925–1940
34. Fang, Y., Li, G., and Ferrie, A. M. (2007) Non-invasive optical biosensor for assaying endogenous G protein-coupled receptors in adherent cells. *J. Pharmacol. Toxicol. Methods* **55,** 314–322
35. Minneman, K. P., Lee, D., Zhong, H., Berts, A., Abbott, K. L., and Murphy T. J. (2000) Transcriptional responses to growth factor and G protein-coupled receptors in PC12 cells: comparison of α_1-adrenergic receptor subtypes. *J. Neurochem.* **74,** 2392–2400
36. Yang, M., Reese, J., Cotecchia, S., and Michel, M. C. (1998) Murine α_1-adrenoceptor subtypes. I. Radioligand binding studies. *J. Pharmacol. Exp. Ther.* **286,** 841–847
37. Ramachandran, R., and Hollenberg, M. D. (2008) Proteinases and signaling: pathophysiological and therapeutic implications via PARs and more. *Br. J. Pharmacol.* **153,** S263–S282
38. Paavola, K. J., and Hall, R. A. (2012) Adhesion G protein-coupled receptors: signaling, pharmacology, and mechanisms of activation. *Mol. Pharmacol.* **82,** 777–783
39. Langenhan, T., Aust, G., and Hamann, J. (2013) Sticky signaling–adhesion G protein-coupled receptors take the stage. *Sci. Signal.* **6,** re3
40. Paavola, K. J., Stephenson, J. R., Ritter, S. L., Alter, S. P., and Hall, R. A. (2011) The N terminus of the adhesion G protein-coupled receptor GPR56 controls receptor signaling activity. *J. Biol. Chem.* **286,** 28914–28921
41. O'Hara, P. J., Sheppard, P. O., Thøgersen, H., Venezia, D., Haldeman, B. A., McGrane, V., Houamed, K. M., Thomsen, C., Gilbert, T. L., and Mulvihill, E. R. (1993) The ligand-binding domain in metatropic glutamate receptors is related to bacterial periplasmic binding proteins. *Neuron* **11,** 41–52
42. Lin, Z., Walther, D., Yu, X. Y., Drgon, T., and Uhl, G. R. (2004) The human serotonin receptor 2B: coding region polymorphisms and association with vulnerability to illegal drug abuse. *Pharmacogenetics* **14,** 805–811
43. Belmer, A., Doly, S., Setola, V., Banas, S. M., Moutkine, I., Boutourlinsky, K., Kenakin, T., and Maroteaux, L. (2014) Role of the N-terminal region in G protein-coupled receptor functions: negative modulation revealed by 5-HT$_{2B}$ receptor polymorphisms. *Mol. Pharmacol.* **85,** 127–138
44. Strasser, A., Wittmann, H. J., and Seifert, R. (2008) Ligand-specific contribution of the N terminus and E2-loop to pharmacological properties of the histamine H1-receptor. *J. Pharmacol. Exp. Ther.* **326,** 783–791
45. Green, S. A., Turki, J., Innis, M., and Liggett, S. B. (1994) Amino-terminal polymorphisms of the human β2-adrenergic receptor impart distinct agonist-promoted regulatory properties. *Biochemistry* **33,** 9414–9419
46. Levin, M. C., Marullo, S., Muntaner, O., Andersson, B., and Magnusson, Y. (2002) The myocardium-protective Gly-49 variant of the β1-adrenergic receptor exhibits constitutive activity and increased desensitization and down-regulation. *J. Biol. Chem.* **277,** 30429–30435
47. Hakalahti, A. E., Vierimaa, M. M., Lilja, M. K., Kumpula, E. P., Tuusa, J. T., and Petäjä-Repo U. E. (2010) Human β1-adrenergic receptor is subject to constitutive and regulated N-terminal cleavage. *J. Biol. Chem.* **285,** 28850–28861
48. Hakalahti, A. E., Khan, H., Vierimaa, M. M., Pekkala, E. H., Lackman, J. J., Ulvila, J., Kerkelä, R., and Petäjä-Repo, U. E. (2013) β-Adrenergic agonists mediate enhancement of β1-adrenergic receptor N-terminal cleavage and stabilization *in vivo* and *in vitro*. *Mol. Pharmacol.* **83,** 129–141
49. Overton, M. C., and Blumer, K. J. (2002) The extracellular N-terminal domain and transmembrane domains 1 and 2 mediate oligomerization of a yeast G protein-coupled receptor. *J. Biol. Chem.* **277,** 41463–41472
50. Pace, A. J., Gama, L., and Breitwieser, G. E. (1999) Dimerization of the calcium-sensing receptor occurs within the extracellular domain and is eliminated by Cys → Ser mutations at Cys^{101} and Cys^{236}. *J. Biol. Chem.* **274,** 11629–11634
51. Schwarz, D. A., Barry, G., Eliasof, S. D., Petroski, R. E., Conlon, P. J., and Maki, R. A. (2000) Characterization of γ-aminobutyric acid receptor GABA$_{B(1e)}$, a GABA$_{B(1)}$ splice variant encoding a truncated receptor. *J. Biol. Chem.* **275,** 32174–32181
52. Andersson, H., D'Antona, A. M., Kendall, D. A., Von Heijne, G., and Chin C. N. (2003) Membrane assembly of the cannabinoid receptor 1: impact of a long N-terminal tail. *Mol. Pharmacol.* **64,** 570–577
53. Dunham, J. H., Meyer, R. C., Garcia, E. L., and Hall, R. A. (2009) GPR37 surface expression enhancement via N-terminal truncation or protein-protein interactions. *Biochemistry* **48,** 10286–10297
54. Marchese, A., Paing, M. M., Temple, B. R., and Trejo, J. (2008) G protein-coupled receptor sorting to endosomes and lysosomes. *Annu. Rev. Pharmacol. Toxicol.* **48,** 601–629
55. Eng, J. K., Jahan, T. A., and Hoopmann, M. R. (2013) Comet: an open-source MS/MS sequence database search tool. *Proteomics* **13,** 22–24

	ADRA1A	
Agonist	**pEC_{50}**	**Max (pm)**
Phenylephrine	-6.34 ± 0.04	367.49 ± 9.56
Cirazoline	-7.38 ± 0.10	413.87 ± 8.41
A61603	-7.38 ± 0.09	385.60 ± 7.43
Naphazoline	-7.03 ± 0.07	295.95 ± 12.46
Synephrine	-4.80 ± 0.12	260.61 ± 22.87
Tetrahydrozoline	-6.36 ± 0.10	225.81 ± 5.39
Methoxamine	-6.05 ± 0.11	255.93 ± 21.39
Oxymetazoline	-7.83 ± 0.08	297.57 ± 8.81

Table S2. Agonist pharmacodynamic properties of ADRA1A-stimulated DMR responses. Agonist stimulated DMR concentration-response curves were constructed for α_{1A}-adrenergic receptor (ADRA1A) expressed in HEK293T cells. Agonist potencies (pEC_{50}) were calculated using the time at which peak DMR response was observed. All data were analyzed with GraphPad Prism and are expressed as mean ± SEM of 3 independent experiments performed with 4 replicates.

TABLE S1. TAP-MS/MS proteomic analysis of ADRA1D NT truncation mutants in HEK293T cells. Data shown include GPCR bait, percent peptide coverage (%Cov), number of unique peptides (#UP), PDZ proteins (PDZ) and non-PDZ proteins (Non-PDZ) detected. *** = no proteins detected.

FIGURE S1. GAPDH immunoblot of SNAP-ADRA1D NT mutant HEK293 cell lysates in Fig 3B. SNAP-gels were transferred to nitrocellulose paper, blotted with anti-GAPDH antibodies (1:2000 dilution), washed, then blotted with anti-mouse LI-COR 680 secondary antibodies (1:5000 dilution) and imaged with LI-COR Odyssey.

FIGURE S2. α_{1A} (ADRA1A) DMR responses stimulated by α_1-adrenergic receptor agonists cirazoline (*A*), A61603 (*B*), naphazoline (*C*), oxymetazoline (*D*), tetrahydrozoline (*E*), synephrine (*F*), or methoxamine (*G*) were quantified as concentrated-response curves (*H*) to calculate potency and intrinsic activity. Data are summarized in Table S2 and are the mean ± SEM of 3 independent experiments performed with 4 replicates.

FIGURE S3. Schematic of ADRA1D plasma membrane localization quantification. (*A,B*) Images were quantified by outlining the cellular membrane based on membrane-targeted YFP localization. (*C*) The intracellular region (excluding membrane) was then outlined and subtracted from the first measurement and normalized to area, representing membrane fluorescence per area unit. (*D,E*) Two representative intracellular regions (distinct from nuclear region) were outlined, quantified, and normalized to area to represent cytosolic fluorescence per area unit. These data were used to calculate the ratio of membrane signal to cytosolic signal per area unit, representing relative enrichment at the membrane. (*F,G*) In a blinded analysis of n = 42 cells, Δ1-91 α_{1D}-AR appears enriched at the cellular membrane compared to WT α_{1D}-AR. All cells were scored as either membrane-positive or membrane-negative and data were graphed as a percentage.

Figure S1 *N-terminal cleavage of α_{1D}-adrenergic receptor*

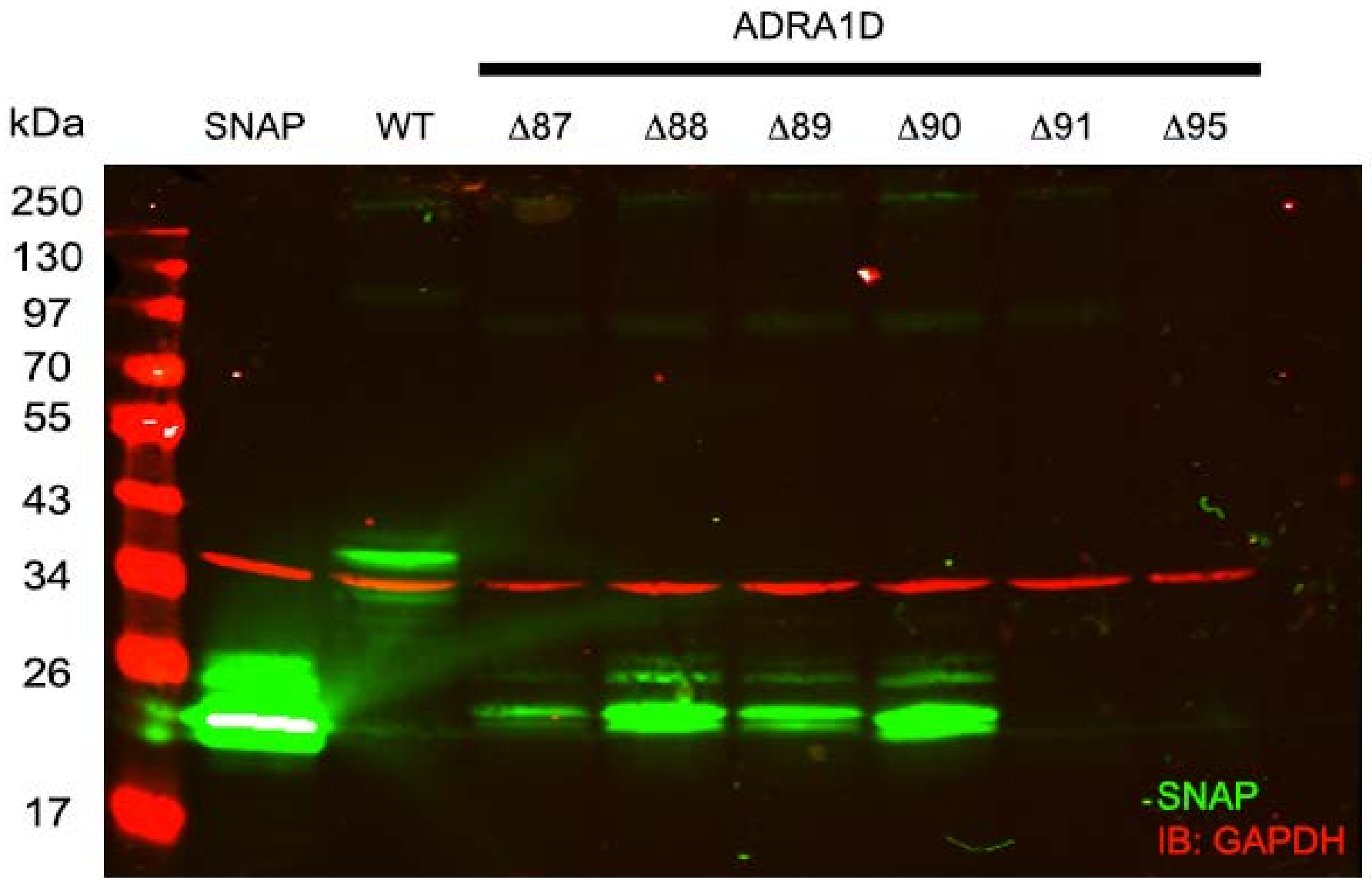

Figure S2

N-terminal cleavage of α_{1D}-adrenergic receptor

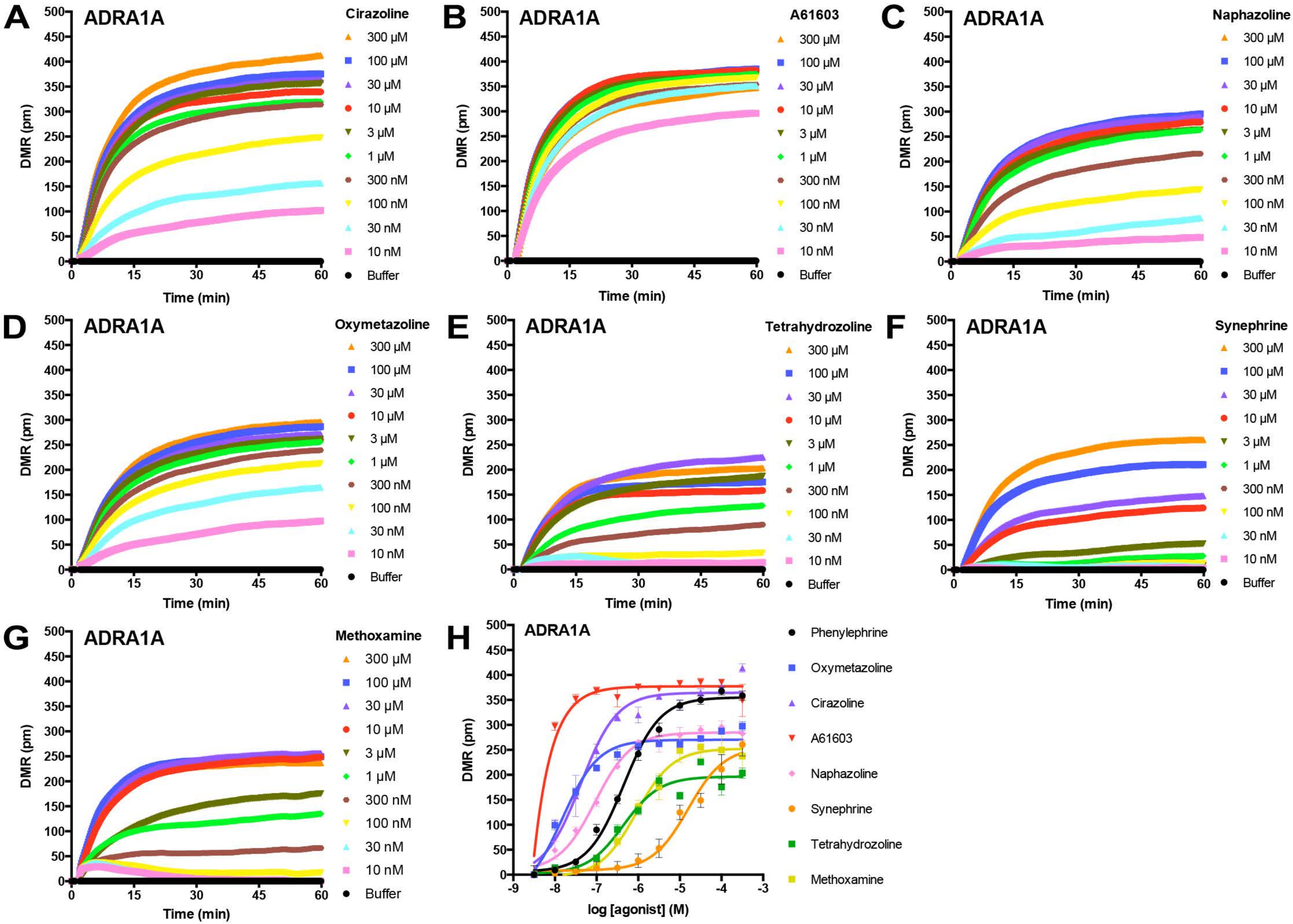

Figure S3 *N-terminal cleavage of α_{1D}-adrenergic receptor*

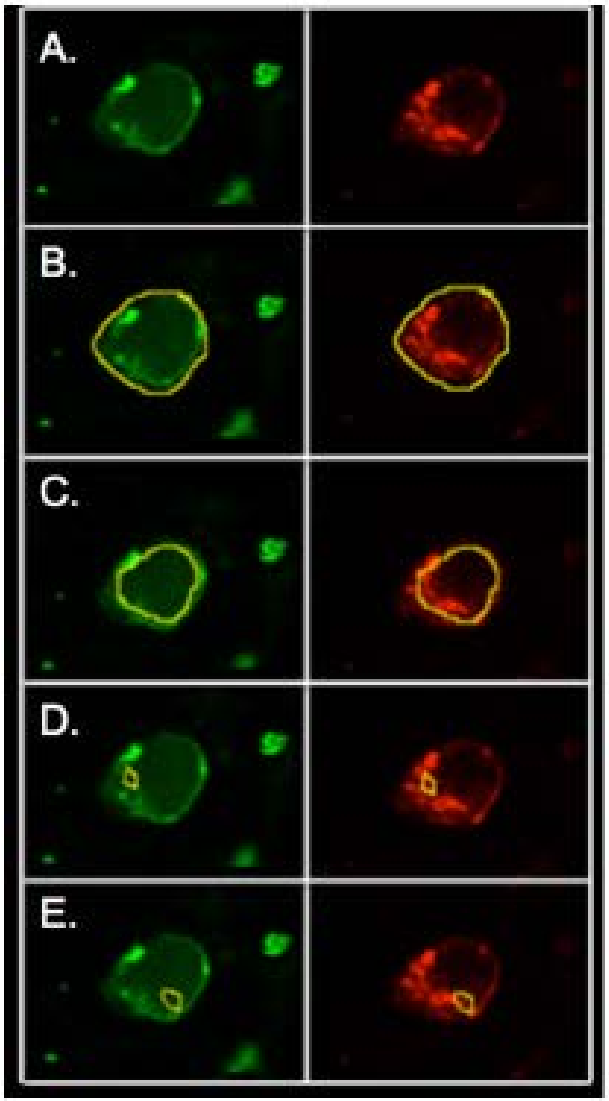

F.

	WT	Δ1-91
Membrane Positive	5	15
Membrane Negative	14	8
Total Cells	19	23
%	26%	65%

G.

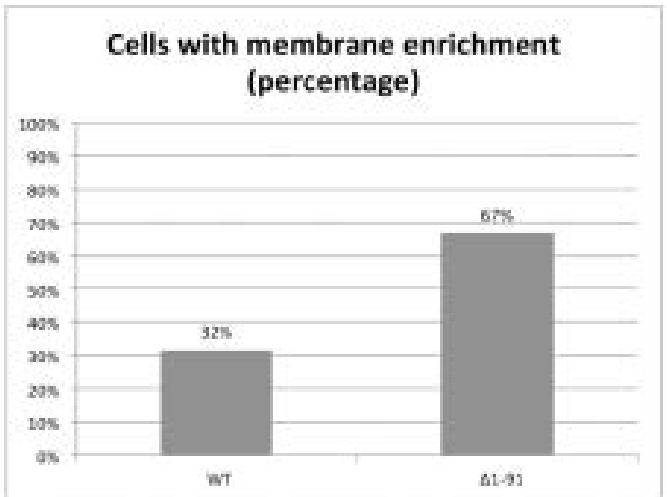

Endogenous N-terminal Domain Cleavage Modulates α_{1D}-Adrenergic Receptor Pharmacodynamics

Timothy S. Kountz, Kyung-Soon Lee, Stacey Aggarwal-Howarth, Elizabeth Curran, Ji-Min Park, Dorathy-Ann Harris, Aaron Stewart, Joseph Hendrickson, Nathan D. Camp, Alejandro Wolf-Yadlin, Edith H. Wang, John D. Scott and Chris Hague

J. Biol. Chem. 2016, 291:18210-18221.
doi: 10.1074/jbc.M116.729517 originally published online July 5, 2016
